Journal of Geophysical Research – Solid Earth

Supporting Information for

GRACE and GRACE Follow-On gravity observations of intermediate-depth earthquakes contrasted with those of shallow events

Shin-Chan Han (1)*, Jeanne Sauber (2), Taco Broerse (3), Fred Pollitz (4), Emile Okal (5), Taehwan Jeon (6), Ki-Weon Seo (6), Richard Stanaway (7)

(1) School of Engineering, University of Newcastle, Callaghan, NSW, Australia

(2) Geodesy and Geophysics Laboratory, NASA Goddard Space Flight Center, Greenbelt, MD, USA

(3) Department of Earth Sciences, Utrecht University, Utrecht, The Netherlands

(4) U.S. Geological Survey, Menlo Park, CA, USA

(5) Department of Earth and Planetary Sciences, Northwestern University, Evanston, IL, USA

(6) Department of Earth Science Education, Seoul National University, Seoul, Korea

(7) Papua New Guinea University of Technology, Lae, Papua New Guinea

*Correspondence to: shin-chan.han@newcastle.edu.au

This file includes:

Supplementary Figure S1 to S7

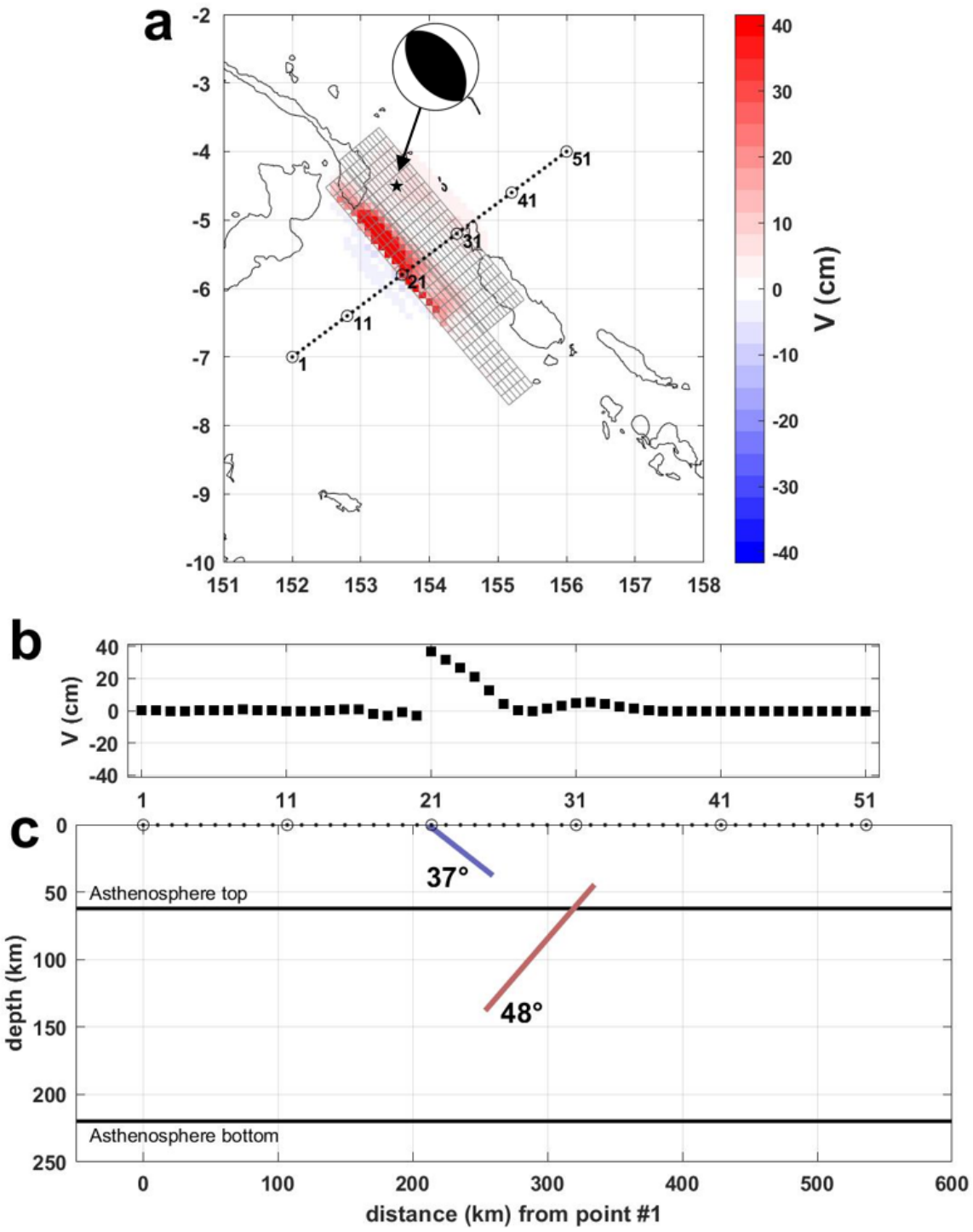

Figure S1. (a) The calculated vertical land motion (VLM) from the USGS finite fault solution of the 2016 earthquake with two fault planes. (b) VLM evaluated over the cross section shown in (a). (c) Two fault planes with dip angles present shallow interface thrusting between two colliding plates and intermediate-depth thrusting within the subducting slab.

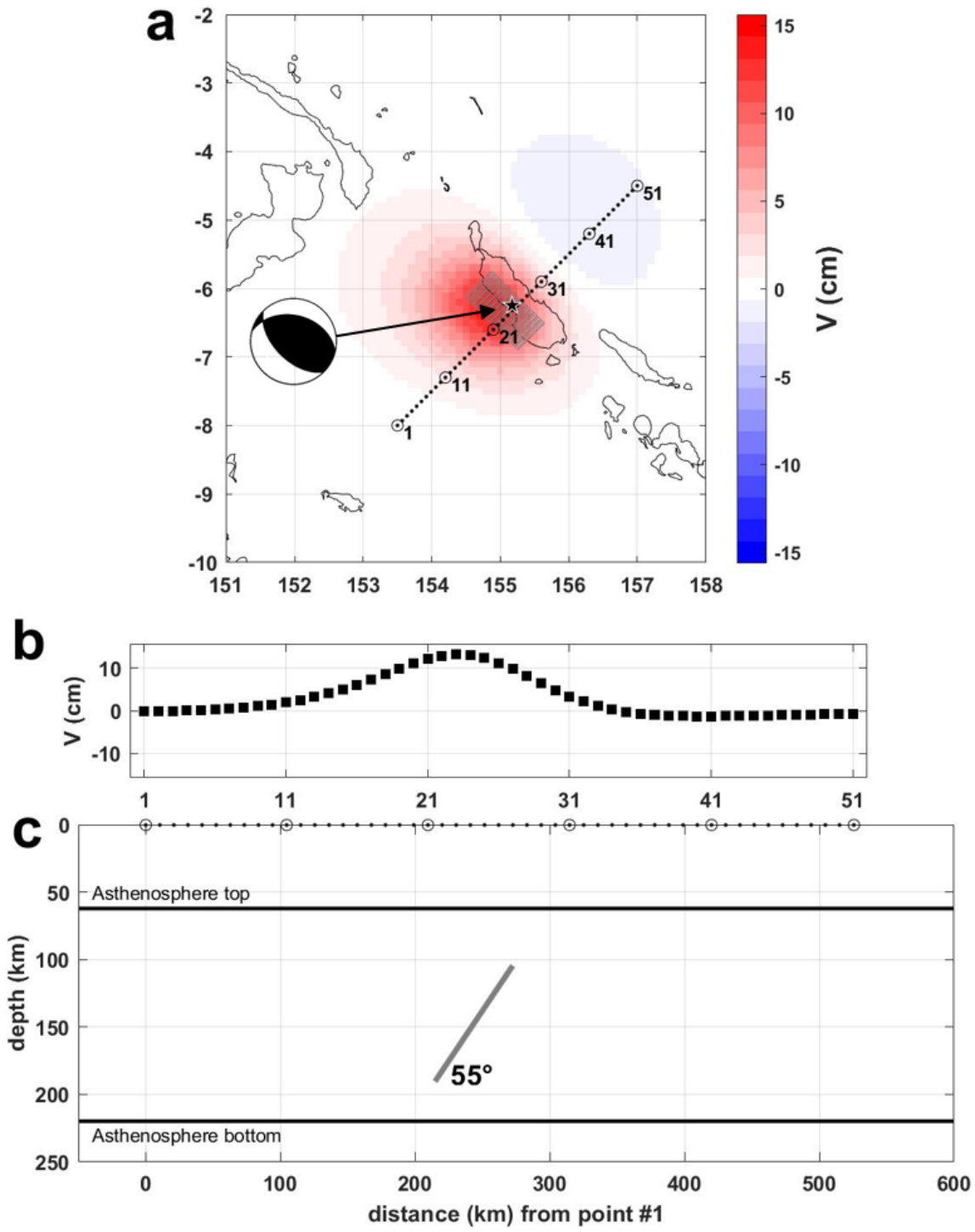

Figure S2. The same as Figure S1 but for 2017 intraslab thrust earthquake at an intermediate depth.

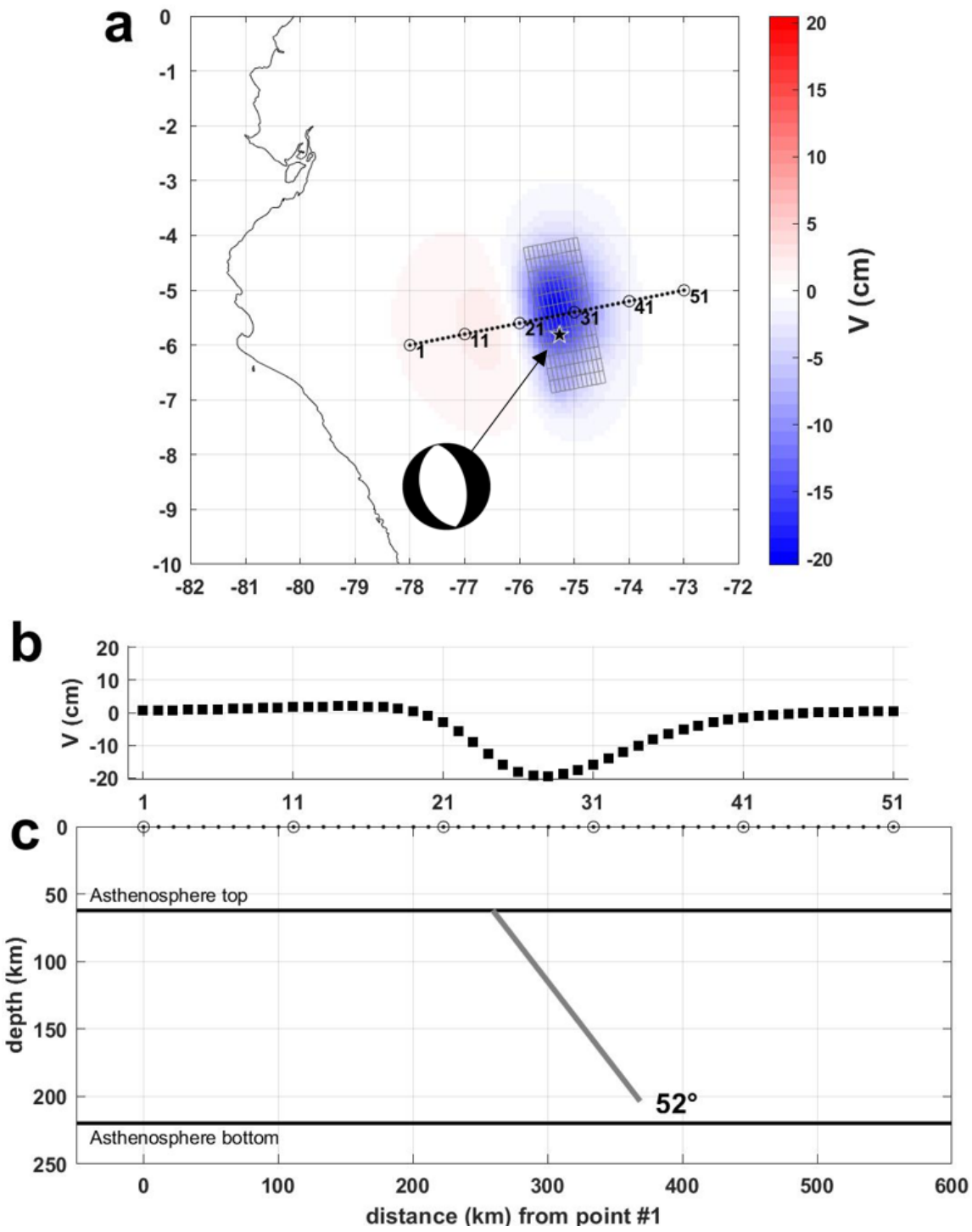

Figure S3. The same as S1 and S2, but from the USGS finite fault model of the normal faulting for the 2019 Peru intermediate-depth earthquake. The predicted spatial pattern of the subsidence, and its falloff, as well as the small uplift in the west, is consistent with GPS measurements in location but smaller in magnitude than the GPS observations.

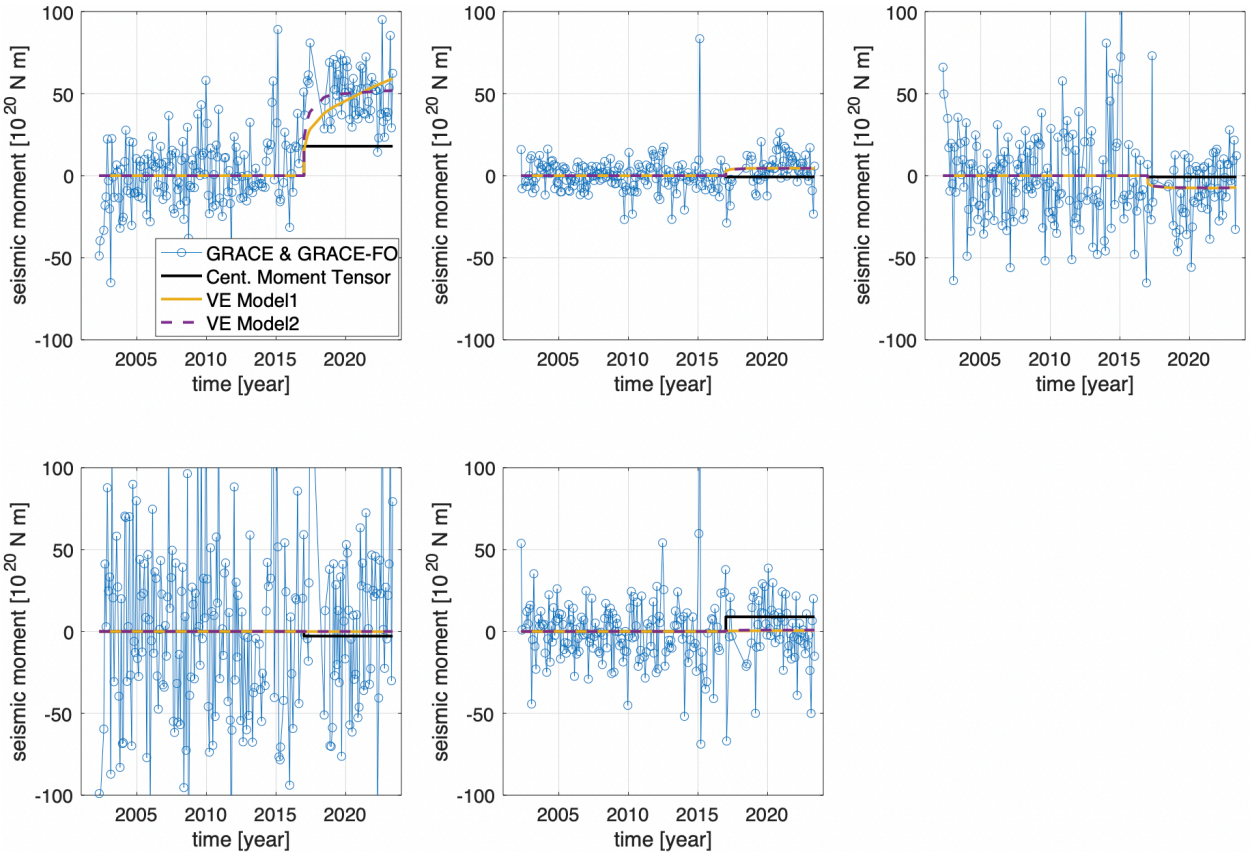

Figure S4. The same as Figure 6 but with the viscoelastic models of (1) VE Model 1: the same lithosphere thickness and the lower asthenosphere steady-state viscosity of 5×10^{18} Pa s (yellow solid curve), and (2) VE Model 2: the thinner lithosphere of 40 km and the same asthenosphere steady-state viscosity of 5×10^{19} Pa s (purple dashed curve).

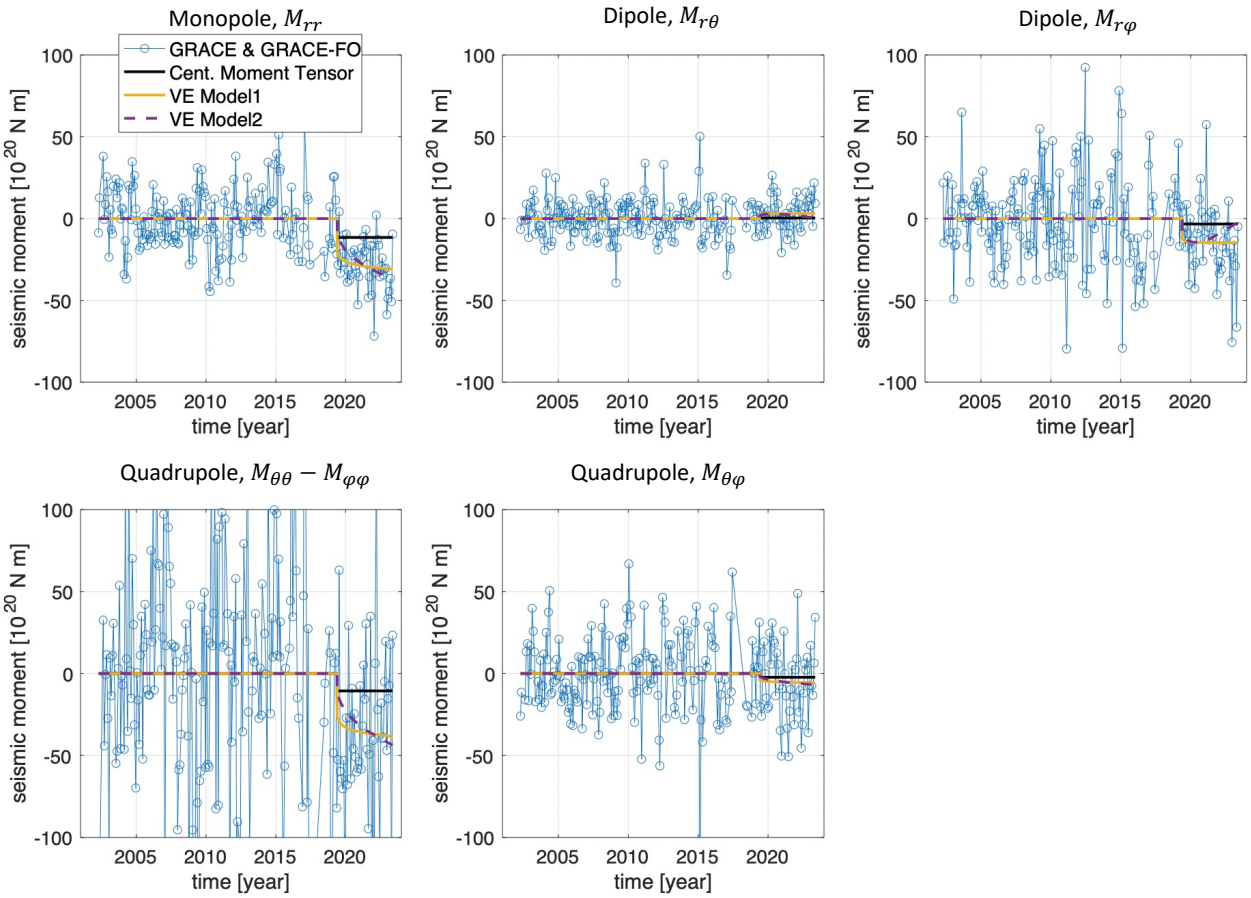

Figure S5. The same as Figure 7 but with the viscoelastic models of (1) VE Model 1: the same lithosphere and the asthenosphere steady-state viscosity of 1×10^{19} Pa s (yellow solid curve), and (2) VE Model 2: the same lithosphere and the lower asthenosphere steady-state viscosity of 5×10^{18} Pa s (purple dashed curve).

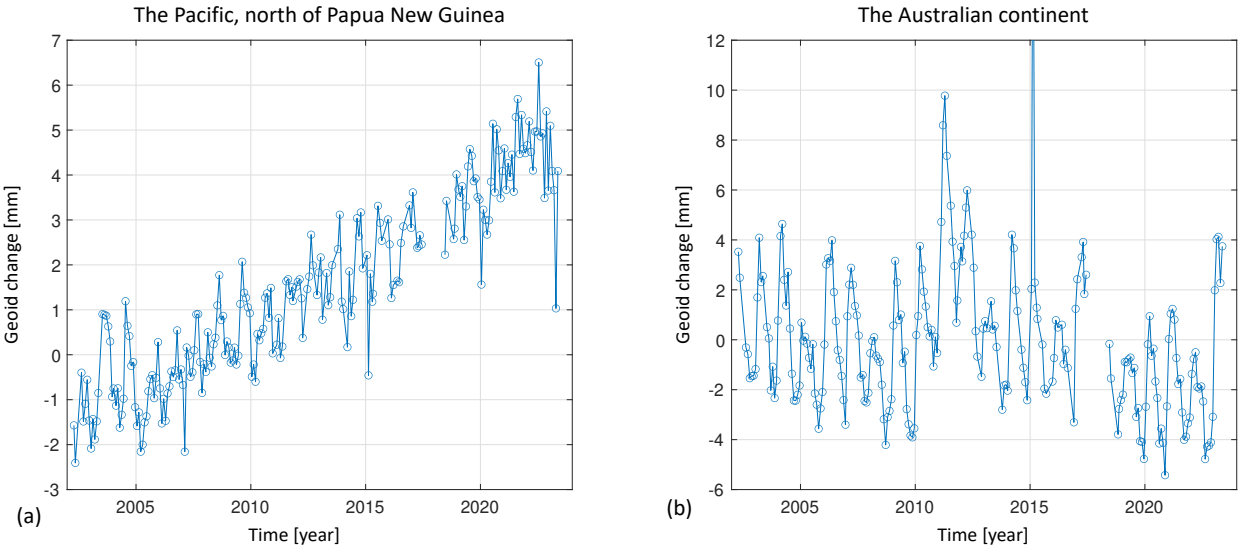

Figure S6. The monthly time series of the geoid change at (a) the Pacific Ocean, north of Papua New Guinea (23°N, 132°E) and (b) the central Australia (21°S, 134°E). Both figures show large geoid change in the geoid difference map of Figure 8a before and after the 2016/2017 earthquakes. However, they are not associated with the earthquake but instead are indicative of ocean mass and land hydrology variation, respectively.

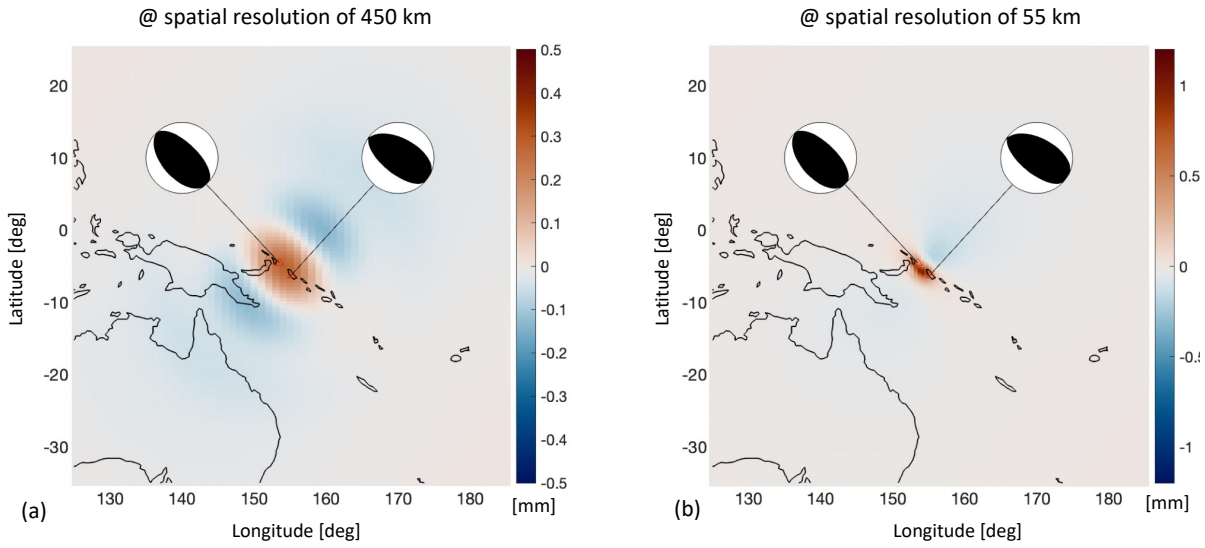

Figure S7. The synthetic geoid change from the seismic finite fault models of the 2016/1017 earthquake at (a) the spatial resolution of 450 km commensurate with the GRACE data as in Figure 8a, and (b) at a higher resolution of 55 km relevant to the local sea level and land deformation measurements (such as GPS). Note that there is insignificant geoid change from the spatial resolution of 110 km and shorter. Therefore, we conclude that the resolution of 55 km is sufficient to represent the local variations.